

Producing Plant Virus Patterns with Defined 2D Structure

Christine Müller-Renno, Diana Rimmel, Mario Braun, Kajohn Boonrod, Gabi Krczal, and Christiane Ziegler*

In nanobiotechnology, viral nanoparticles have come into focus as interesting nano building blocks. In this context, the formation of 2D and 3D structures is of particular interest. Herein, the creation of defined 2D patterns of an icosahedral plant virus, the tomato bushy stunt virus (TBSV), by means of different techniques is reported on: the top-down lithography ebeam and focused ion beam (FIB) as well as the bottom-up fluidic force microscope (FluidFM) approach. The obtained layer structures are imaged by scanning force and scanning electron microscopy. The data show that a defined 2D structure can successfully be created either top down by FIB or bottom up by FluidFM. Electron beam lithography is not able to remove viruses from the substrate under the chosen conditions. FIB has an advantage if larger areas covered with viruses combined with smaller areas without being desired. FluidFM is advantageous if only small areas with viruses are required. A further benefit is that the uncovered areas are not affected. The pattern formation in FluidFM is influenced not only by the spotting parameters, but in particular by the drying process. Deegan and Marangoni effects are shown to play a role if the spotted droplets are not very small.

Lithographically guided self-organization processes such as the imprint technique combine the two different approaches.

Nanobiotechnology requires pattern formation of biological building blocks, such as proteins, DNA, or virus particles. Proteins, e.g., offer a wide range of structural and functional properties and thus have a huge potential for applications, e.g., in the field of enzymatic assays with controlled spatial protein arrangement.^[4,5] Protein assemblies are furthermore ideal templates to form regular 1D, 2D, and 3D superstructures. Virus nanoparticles (VNPs) and virus-like particles (VLPs, which lack genetic information and are thus noninfectious) are popular protein-based objects for self-assembly in a bottom-up approach.^[6–10] Their main advantages are their perfectly uniform size and their easy modification through genetic modification, which allows, e.g., a


1. Introduction

The creation of nanopatterns has been the subject of intensive research for decades. Often, two different approaches are distinguished: top-down and bottom-up.^[1–3] In the former, pattern formation is achieved through lithographic processes, in which the negative of the desired structure is removed from a closed layer (2D) or massive material (3D). Methods such as focused ion beam (FIB) and electron beam lithography are successfully used here.^[1–3] In the bottom-up approach, nanostructures are assembled from individual components through self-organization.^[1–3]

homogeneous coverage with specific peptide chains. Furthermore, such plant viruses are produced by sustainable green technology, i.e., in greenhouses. Their application ranges from material fabrication to biosensor technology and biomedical applications.^[11–15] The layer systems are mostly based on self-assembly and the viruses or VLPs interact via electrostatics or functional groups.^[16,17] Through a clever choice of Coulomb forces or the use of functional units, both 2D and 3D assembly on solid supports can be controlled and optimized.^[10,18] For more complex applications such as microarray-based assays or nanomachines, laterally defined patterns are required, such as squares, rectangles, or circles. However, common methods to apply virus particles, e.g., spin coating, dip coating, and drop and dry,^[18–20] are per se not suitable for directed pattern formation. In contrast, fluidic force microscopy (FluidFM, a type of scanning force microscopy (SFM)) allows local liquid dispensing and therewith writing respectively printing in the range of nanometers.^[21–23] This is possible through the handling of small liquid volumes (femtoliter) via nanofluidic channels in the cantilevers.^[22,24] Applying an overpressure to the microchanneled cantilever leads to the deposition of the desired material (liquids or nanoparticles), while the feedback of the scanning force microscope regulates the contact between the nanopipette respectively nanosyringe with the substrate. (In addition to the here-utilized mode of spotting, FluidFM can also be used for a variety of applications, such as immobilizing soft colloidal particles^[25,26] or cells^[27,28] at the tip for single-particle or single-cell force spectroscopy by an underpressure, producing

C. Müller-Renno, D. Rimmel, C. Ziegler
Department of Physics and Research Center OPTIMAS
University of Kaiserslautern
Erwin-Schrödinger-Str. 56, Kaiserslautern 67663, Germany
E-mail: cz@physik.uni-kl.de

M. Braun, K. Boonrod, G. Krczal
AlPlanta - Institute for Plant Research
RLP Agroscience GmbH
Breitenweg 71, Neustadt a. d. Weinstraße 67435, Germany

 The ORCID identification number(s) for the author(s) of this article can be found under <https://doi.org/10.1002/pssa.202100259>.

© 2021 The Authors. *physica status solidi (a) applications and materials science* published by Wiley-VCH GmbH. This is an open access article under the terms of the Creative Commons Attribution License, which permits use, distribution and reproduction in any medium, provided the original work is properly cited.

DOI: 10.1002/pssa.202100259

controlled nanopores to suck material out of single cells^[27] or to measure the activity of single ion channels,^[29,30] and applying specific drugs or interaction partners at specific sites or into selected single cells.)^[27,31]

We here report on the formation of specific patterns of genetically modified tomato bushy stunt virus (TBSV) particles. TBSV has a stable icosahedral shape, a diameter of 30 nm, and shows extreme robustness. The viral capsid counts 180 subunits and offers a variety of possibilities to introduce biologically and chemically interesting units such as peptides on the subunits of the capsid.^[32,33] In addition, the icosahedral shape offers a high degree of symmetry.^[34–36]

In former work, we report on the preparation of highly ordered 2D virus layers,^[18–20] and in a recent publication,^[10] we were able to show the first controlled virus bilayers. As the next step, defined 2D patterns such as dots, rings, and squares are required, which can then serve as a basis for real 3D structures such as a virus nanoactuator. These 2D patterns can either be spontaneously formed, e.g., by mixing rod-and-ball-shaped viruses, which will be reported elsewhere. The more laborious but also more versatile methods for a directed formation of predefined structures will be discussed here. We compare a recent direct writing method utilizing FluidFM^[37,38] with more classical particle beam lithography, i.e., electron beam and focused ion beam lithography. FluidFM spotting was optimized by systematically varying parameters such as virus concentration, overpressure, and setpoint force. The quality of the individual viral structures and viral-free areas was examined using both SFM and scanning electron microscopy (SEM).

2. Experimental Section

2.1. Genetic Modification of TBSV VNP

Genetically modified TBSV particles (decorated with 4D6H and Strep-tag peptides) were generated as described by Lüders et al.^[19] using the primers described in the **Table 1**. The in vitro transcribed RNAs of the different derivatives were inoculated onto *Nicotiana benthamiana* plants. The virus particles were purified from the infected plants as described by Lüders et al.^[19] The purity of virus particles was confirmed by sodium dodecyl sulfate polyacrylamide gel electrophoresis (SDS-PAGE) and the concentration was measured by Bradford reagent (BioRad).

2.2. Materials

For the FluidFM, microscope slides made from borosilicate glass (hydrolytic class 1, Paul Marienfeld, Germany) were used as substrates. They were cleaned by a standard cleaning process with

subsequent immersion in acetone, isopropanol, and water in an ultrasonic bath (each 10 min) and were then activated by oxygen plasma (50 W, 10 sccm O₂, 5 min). The substrates were directly used after the cleaning process.

Substrates for the electron and focused ion beam methods were pieces of silicon wafers (Si-Mat, Germany) with a crystal orientation (100) (native oxide, orientation specificity $\pm 0.5^\circ$, thickness 500–550 μm , one side polished, type p, boron-doped, specific resistance 1–5 $\Omega\text{ cm}$). They were cleaned two times by the aforementioned standard cleaning process. Afterward, the substrates were dried in a nitrogen flow and directly used.

The virus stock solutions (4D6H TBSV, respectively, Strep-tag TBSV) were diluted with 0.02 M sodium acetate buffer (pH 5.2) to the desired final concentrations, which are mentioned in the corresponding results part. The quoted concentrations are the mass concentrations of the coat protein (CP), which are proportional to the virus concentrations.

Mixtures of virus solution with glycerol (Sigma Aldrich, Germany) were utilized for several reasons (see part III.). The contact angle of the final virus glycerol mixture (final virus concentrations 0.5 and 1.0 $\mu\text{g}\ \mu\text{L}^{-1}$, respectively) was measured (G2 contact angle measurement system, Krüss, Germany). The contact angles lie in the range of 8–10° and are comparable within their error bars. In addition, the viscosities were measured with Viscometer DV3T extra (Brookfield, USA). Also here, no differences for both concentrations were detected. However, the virus solution without glycerol had a substantially different viscosity of ≈ 1.1 mPas compared to those with glycerol (6.4–6.8 mPas).

2.3. Layer Preparation and 2D Structuring

Closed viral layers on silicon for subsequent focused ion/electron beam lithography were produced by means of a spin coater as described in Rink et al.^[20] In short, a droplet of 5 μL Strep-tag II TBSV (1.0 $\mu\text{g}\ \mu\text{L}^{-1}$) solution was placed in the middle of the silicon plate and then rotated at 2000 rpm with an acceleration of 3000 rpm s⁻¹ for 200 s at a relative humidity of 50.4% and $T = 18.4^\circ\text{C}$.

FIB (FEI Stata400 DualBeam, USA) lithography was performed at the Institute for Surface and Thin Film Analysis (IFOS, Kaiserslautern). A gallium ion beam at an acceleration voltage of 30 kV and an aperture giving a sample current of 0.92 nA for the circles and 2.8 nA for the squares (gallium ion beam), respectively, was used.

Electron beam lithography (e_Line-System, Raith, Germany) was performed at the Nano Structuring Center of the TU Kaiserslautern. The parameters used were 0.17 nA electron beam current at an acceleration voltage of 20 kV and different exposure times resulting in exposure doses of 500 $\mu\text{C cm}^{-2} \times 1, 2.24, 8, 16, 32, 64, 128, 256, \text{ and } 512$.

Table 1. Primers used for TBSV.

Primer name	Purpose	Sequence (5' -> 3')
CPP6	General TBSV forward	GACATCTGGATCTGTAC
Rev 4D6H Stop Xhol	4D6H peptide sequence	CCTCGAGTTAGTGATGGTGATGGTGATGATCATCATCGAGTAAGTTAAACAACATTAGCTCC
Rev TBSV Strep Xhol	Strep Tag sequence	CCTCGAGTTAGTGATGGTGATGGTGATGATCATCATCGAGTAAGTTAAACAACATTAGCTCC

All bottom-up spotting experiments were performed with a Nanowizard III scanning force microscope (JPK Instruments AG, D), assembled with a FluidFM add-on (Cytosurge, Switzerland), positioned under an acoustic hood (JPK Instruments AG, D), and mounted on an active vibration isolation system (Halcyonics-i4, Accurion GmbH, Germany) to minimize the effects of environmental vibrations. For the spotting process, a FluidFM nanopipette and nanosyringe (both Cytosurge, Switzerland), respectively, were filled with the viral solution by applying a pressure of 1000 mbar. Subsequently, several structures were placed on a glass slide using different parameters as given in Section 3 (see **Figure 1**). The spotted structures were then dried overnight at room temperature (23–24 °C) and relative humidity of $\approx 35\%$. The FluidFM was used in the single force-distance curve mode. Here, the cantilever is moved in the *z*-direction to the surface, is pressed on it for the desired time at the desired force (setpoint or dwell force), and afterward, the cantilever is retracted from the surface. The nanopipettes had a spring constant of 0.6 N m^{-1} and a mean aperture of 300 nm. The nanosyringes had a spring constant of 2.2 N m^{-1} and a nominal aperture of 600 nm. The nanopipette and the nanosyringe differ concerning the position of the aperture (see **Figure 1**). Whereas the aperture of the nanopipette is circular and situated at the tip apex, the nanosyringe has an opening at the lowest part of the back of the pyramidal tip. Liquid from the nanopipette is hence spotted underneath the tip, from the nanosyringe behind the tip.

In some cases, preparation of the FluidFM cantilevers was performed. This is described in the Supporting Information.

2.4. Microscopy

The surface topography was investigated with a Nanowizard 3 scanning force microscope (JPK, Berlin) in QI mode and a multimode, respectively, and with a Nanoscope 3a Controller (Digital Instruments, USA) in tapping mode, both in air. QI mode is a force–distance-curve-based imaging mode that delivers nanomechanical properties as well as height and topography information during the same run.

During tapping mode, microcantilevers of the Olympus OMCL-AC100TS-R3, resonance frequency 300 kHz, spring constant 26.1 N m^{-1} with a tip radius of less than 10 nm, were applied.

For QI imaging, cantilevers of μ -Masch (CSC37/No Al with a resonance frequency of 40 kHz and a spring constant of 0.8 N m^{-1}) and Budget Sensors (ContAL-G cantilevers with a resonance frequency of 13 kHz and a spring constant of 0.2 N m^{-1}) were used.

The scanning electron microscope images were recorded with a Hitachi SU8000 at the Nano Structuring Center of the Technical University of Kaiserslautern. Prior to the measurement, the nonconductive viruses were placed in a high-vacuum coating system (Leica EM ACE600) and coated with an $\approx 2 \text{ nm}$ thick conductive iridium layer.

The surface coverage was determined using the histogram function in the software SPIP (scanning probe imaging processor, Image Metrology). In the histogram function, the number of counts is plotted against the height measured in the image. By choosing the cursor position, the area covered with viruses can be distinguished from the uncovered surface area. The given surface coverage here is the ratio between virus-covered areas and the whole imaged area.

3. Results and Discussion

To create viral templates with defined 2D structures, we followed two different approaches. The first one is a bottom-up approach. The structures are written by means of spotting with the FluidFM. The second one starts with an extended monolayer of viruses. Subsequently, the structures are formed in a top-down approach by removing the viruses between the desired structures by electron and ion beam lithography.

3.1. Spotting Viral Patterns with the FluidFM

In the following, virus patterns obtained by spotting with the FluidFM are presented. Technically, spotting utilizes force–distance curves. During the contact or dwell time, pressure is applied to release the fluid.

In FluidFM spotting, several parameters have to be optimized to reveal optimal results, namely, the size and the position of the pipette/syringe opening, the concentration of the spotted material, here the viruses, the amount of glycerol additive (see later), the pressure by which the drops are released from the pipette/

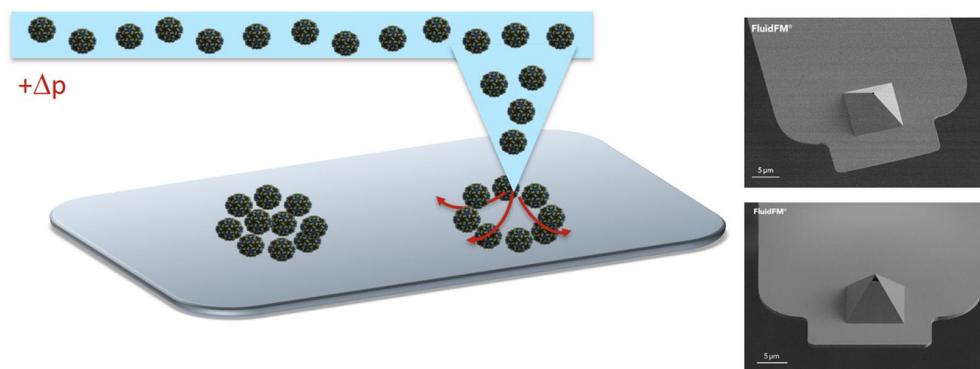


Figure 1. Scheme of the spotting process with the FluidFM (left). SEM images of the nanopipette (upper right) and the nanosyringe (lower right). Image courtesy of Cytosurge AG.

syringe, and the setpoint (dwell force) and dwell time, by which the pipette/syringe is pressed onto the surface during the spotting process.

For more complex structures such as squares and rectangles, the FluidFM is operated in contact mode with a scanning tip or in force–distance curves mode by working in a grid. Here, also speed and proper choice of the writing process have to be controlled.

Herein, the parameters dwell force, virus concentration, glycerol virus mixture ratio, and applied pressure were examined for a spotting process with nanosyringes.

The use of nanopipettes resulted in worse results, which are shown in the Supporting Information. Writing complex structures by scanning has not revealed intact viruses so far, but will be further examined.

The used dwell time for all the experiments was 1 s. In all cases, glycerol was added to the virus solution. This has the advantage that it prevents the nanosyringe from drying out, which can therefore be used more often. It also changed the viscosity of the liquid and thus the spotting process. In addition, it influences the drying process after spotting because glycerol has a lower evaporation rate than water.

In the first experiment, the release pressure was varied (20, 50, 100, 1000 mbar). The other parameters were kept constant: A nanosyringe was filled with a glycerol virus solution mixture at a ratio of 1:1, giving a final virus concentration of $0.5 \mu\text{g} \mu\text{L}^{-1}$. This concentration was chosen because it gave monolayer coverages with not too dense viral patterns in the alternative spin-coating process.^[39] The setpoint was set to 10 nN. In all spotted drops, islands composed of intact viruses can be found. The viruses appear as round-shaped objects with a diameter of about 30 nm and arrange in monolayers with a few bilayer spots. This appearance is the same as in layers produced by spin coating without glycerol additive;^[10,18–20] i.e., there is no apparent effect of glycerol on the viruses.

As can be derived from **Figure 2**, the applied pressure has a markable influence on the obtained virus coverages. The surface coverage (determined in the zoomed images in **Figure 2**, right column) increases from 40.3% at 20 mbar to 75.2% at 50 mbar, 76.1% at 100 mbar, and 83.4% at the highest pressure of 1000 mbar; i.e., we see a nearly constant coverage above a pressure of 50 mbar.

In the second set of experiments, the final virus concentration was increased to $1.0 \mu\text{g} \mu\text{L}^{-1}$, again at a ratio of 1:1 (glycerol: virus solution), and a pressure of 0 mbar was applied. The idea to use this pressure was to receive similar (or even higher) coverages with minimized influence on the viruses. The pressure was kept constant and the dwell force during the force–distance curves was varied.

In principle, the dwell force should have only a minor influence if nanosyringes are applied, because the opening has no direct contact with the substrate. This is different if nanopipettes are used. Grüter et al. found that for nanopipettes the dwell force influences the surface coverage with nanoparticles.^[23] For lower dwell forces (<10 nN), the applied pressure was enough that the nanoparticles were able to overcome the dwell force between the opening of the nanopipette and the substrate. For higher dwell forces the nanoparticles were not able to overcome this contact force.

To exclude other effects due to the dwell force, we changed the dwell forces to 5, 10, 15, and 20 nN. The results are shown in **Figure 3**. It can be seen that in our experiment with the

nanosyringe the setpoint has an unexpected influence on the structure. From 15 nN dwell force on to higher values, it can be seen that so-called coffee ring structures (see below) with a dot in the middle are established. The patterns for 15 and 20 nN do not differ in size. Only the width of the ring is not constant at 15 nN. The coffee ring is, however, less intact for the lower dwell forces (5 and 10 nN). One might assume that the missing part of the ring can be found at the inner rim of the intact ring, perhaps due to an inhomogeneous drying process. The reason for this is still unclear.

A zoom into three different regions of the 20 nN structure reveals intact virus patterns in all cases (see **Figure 4**). The surface coverage with viruses differs depending on the position in the drop as is typical in a coffee ring structure in colloidal systems (see later).

As a third experiment, the pressure was now increased at the optimized concentration and setpoint to see whether again a higher coverage could be obtained. **Figure 5** shows that higher pressure again increases the surface coverage. In addition, the diameter of the pattern itself differs and is much higher for 100 mbar. In further experiments, it has to be revealed whether higher applied pressure is uncritical, or whether there is an effect on the attached protein tags which may prevent their recognition in the course of attaching a second virus layer as discussed in Müller-Renno et al.^[10]

In the following, the formation of the different observed patterns, i.e., a more uniform distribution in **Figure 2** and coffee ring structures with (**Figure 3** and **4**) and without a central dot (**Figure 5**) will be briefly discussed. Virus-containing solutions can be treated as so-called nanofluids, well known in colloidal sciences (for a review, see Zhong et al.^[40]). At deposition, the wetting behavior determines the size and shape of the nanofluid drop on the substrate. Here, the wetting behavior and the viscosities of the used solutions are similar and therefore should not lead to the different observed patterns.

After deposition, the drying process of the droplet is responsible for pattern formation. It depends on the evaporation of the fluid on the one hand and particle movement (and final attachment) on the other hand. TBSVs can be considered nanoparticles with a diameter of about 30 nm and are treated as large nanoparticles (several tens of nanometers), which tend to form coffee ring structures if compared to small nanoparticles (of a few nanometers).^[41] Thus both the fluid and the nanoparticles determine the formed pattern, together with the ambient conditions. This includes particle size, particle–particle interactions, particle–substrate interaction, particle concentration, droplet size, evaporation rate, wetting behavior, substrate temperature, and ambient conditions (see, e.g., Zhong et al. and Sadek et al.^[40,42]). Evaporation is often discussed in terms of the motion of the three-phase contact line, whereas the parameters in the droplet and between the droplet and the substrate can be described by the Derjaguin, Landau, Verwey, Overbeek (DLVO) theory.^[43] During the drying process, nanoparticles are moving, in addition to Brownian motion and gravity. The most important flow was first described by Deegan.^[44] It describes a radial movement of the particles to the contact line of the drop due to the higher evaporation rate at the rim of the drop. In consequence, particles from the inner drop stream to the outer rim. If the Deegan flow is dominant during drying, coffee ring structures are obtained.

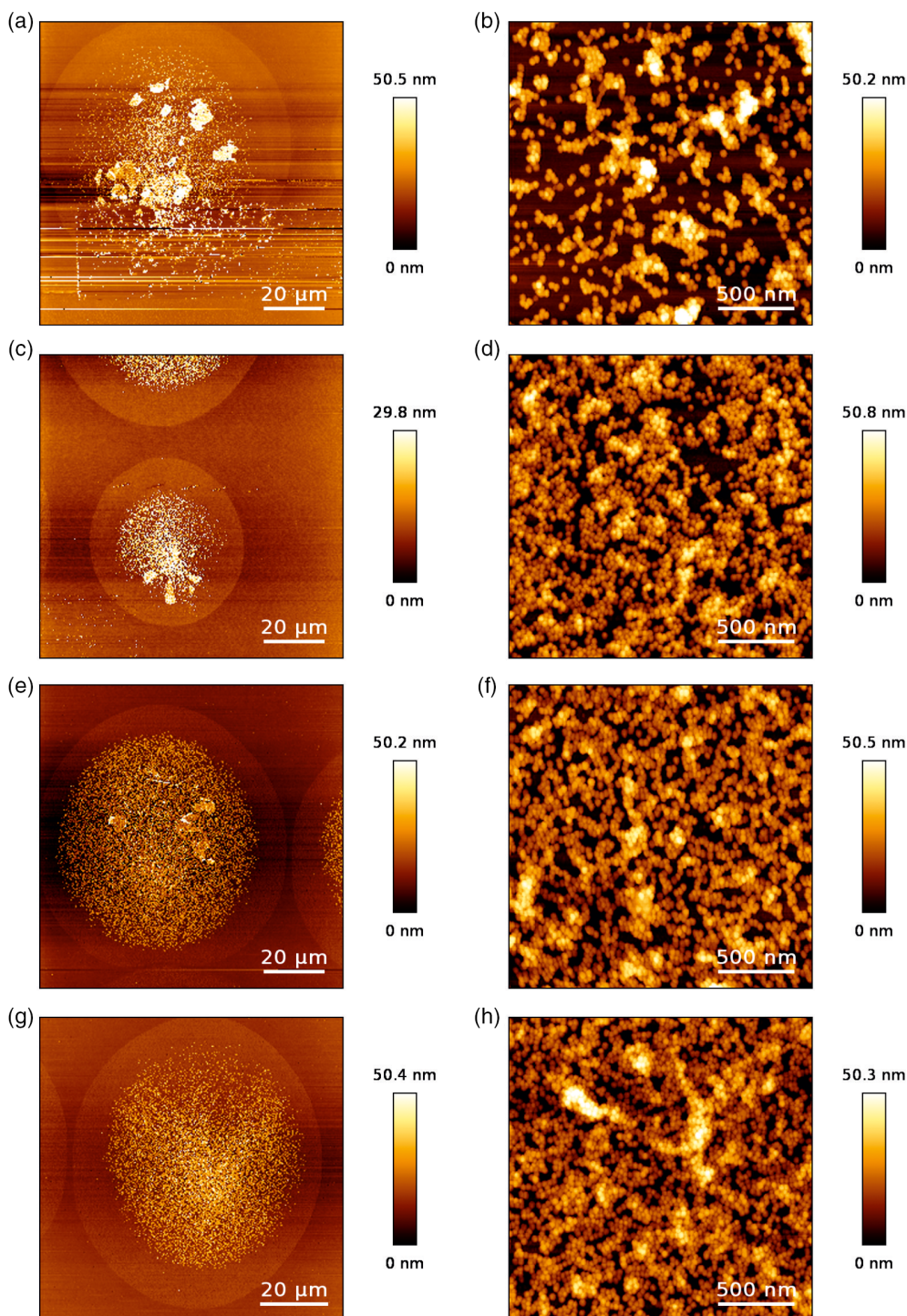


Figure 2. QI-Image of the dots obtained with the nanosyringe filled with the glycerol–water mixture (final 4D6H TBSV concentration: $0.5 \mu\text{g } \mu\text{L}^{-1}$). a,b) @ 20 mbar, surface coverage 40.3%. c,d) @ 50 mbar, surface coverage 75.2%. e,f) @ 100 mbar, surface coverage 76.1%. g,h) @ 1000 mbar, surface coverage 83.4%. All images on the right are zoomed into the center of the corresponding spot on the left side.

It was, however, found that for small drops evaporation may be so fast that the particles do not have time to follow the flow to the contact line, and hence homogeneous spots are formed, although Deegan forces may occur on a longer time scale.^[40]

Another effect, the Marangoni movement, defines streaming of the particles from the drop surface to the inner drop due to locally different surface tensions at the drop surface. It can appear due to concentration differences as well as temperature gradients,

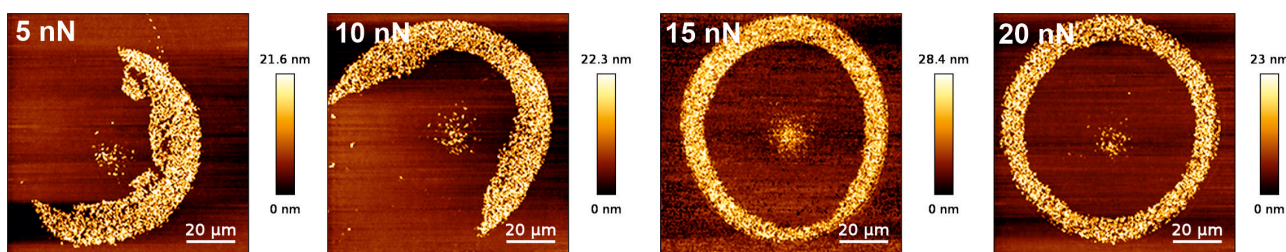


Figure 3. Obtained 4D6H TBSV ($1.0 \mu\text{g} \mu\text{L}^{-1}$) structures as a function of the dwell force: 5 nN (left), 10 nN (center left), 15 nN (center right), and 20 nN (right).

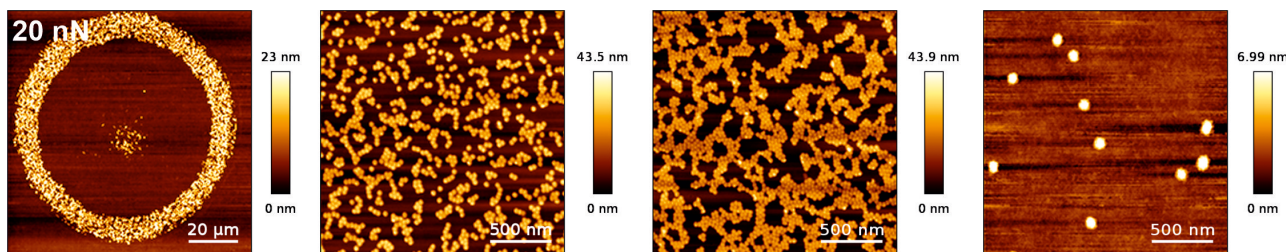


Figure 4. A droplet (4D6H TBSV at $1.0 \mu\text{g} \mu\text{L}^{-1}$), spotted with 20 nN dwell force at 0 mbar pressure. Left: overview; center left: zoom into the central spot; center right: zoom into the outer ring; right: zoom into the region between the central spot and the outer ring.

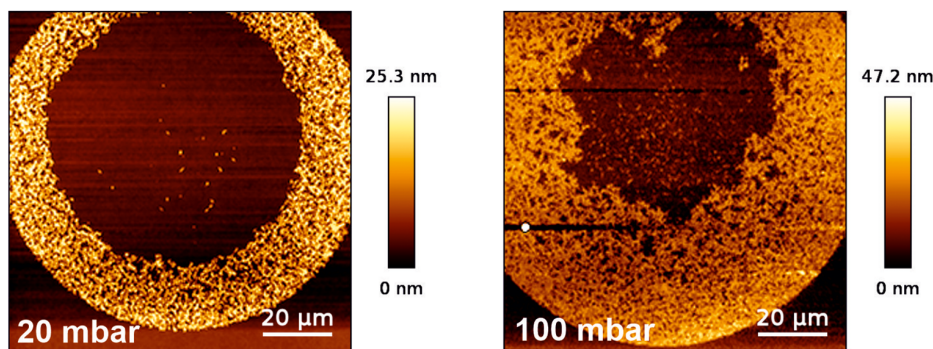


Figure 5. Spotted droplets (4D6H TBSV at $1.0 \mu\text{g} \mu\text{L}^{-1}$) at 20 nN dwell force but different applied pressures: 20 mbar (left) and 100 mbar (right).

both of which can occur in our system because we work not in pure water but in water and glycerol mixtures. The Marangoni effect drives the particles to the center of the drop, in contrast to the Deegan flow. It thus also leads to spots in the center.^[40]

All these parameters together determine whether a coffee ring pattern with or without a central dot or a uniform distribution of the nanoparticles is observed.

As can be determined from Figure 3–5, Deegan flow is apparently the dominant force under these conditions. However, the presence of the small dot at the position of the tip could be due to the counteracting Marangoni effect in Figure 3 and is a result of a far-from-equilibrium process. For conditions as used in Figure 2 (lower concentration) and Figure S3, Supporting Information (nanopipette instead of nanosyringe), smaller droplets are formed and thus evaporation is too fast to allow for coffee ring formation.

In summary, we could show that by varying the drop size (and thus evaporation rate), virus concentration, release pressure, and setpoint force, either spots or rings or both are formed and the filling factor of the rings can be controlled. It is a delicate balance

between many parameters, which is not easy to control. Modeling may be helpful for this purpose.

3.2. Structuring Using a Focused (Ion/Electron) Beam

Whereas FluidFM is a relatively cheap and easy to use addition to an SFM, focused ion beam (FIB) and electron beam (e-beam) lithography require complex and expensive equipment. However, there exists a long tradition and high expertise in lithographic processing by e-beam and FIB, which can be used also in nanobiotechnology. For that purpose, at first, a closed virus layer has to be prepared according to Hiller et al.^[20] (Comment: There is no difference between 4D6H TBSV and Strep-tag II TBSV with respect to the structuring processes reported here.)

In **Figure 6**, SEM images of structures subsequently produced by FIB are shown. The viruses have been removed from the inside of the squares and circles. The virus structure is still

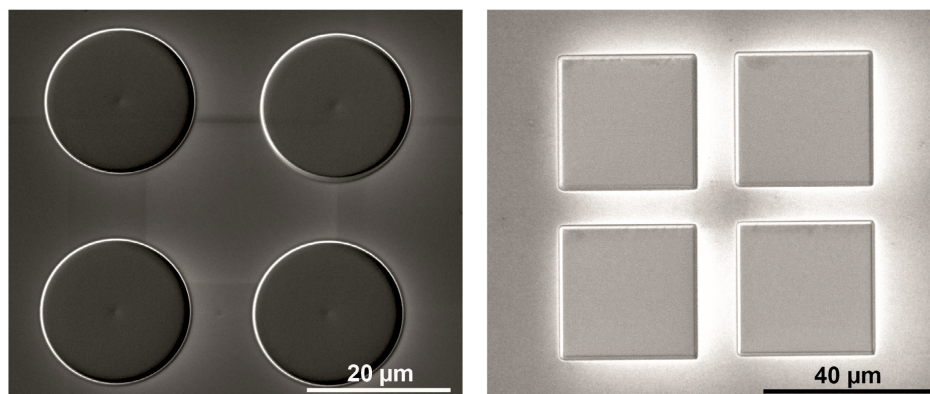


Figure 6. Images of circles and squares written with the focused ion beam into $1.0 \mu\text{g } \mu\text{L}^{-1}$ Strep-tagII TBSV.

present around the squares/circles. It can be seen that FIB allows the creation of different shapes of patterns without any additional effort.

To be sure that the viruses were destroyed by interaction with the focused ion beam, the samples were examined in intermittent mode with a scanning force microscope. In each case, positions within the structures, right next to the structures, and at a greater distance to the structures were imaged. The latter recordings served as a reference to see whether the remaining virus layer survives the writing process unscathed. In **Figure 7** images of the various locations in the virus layer are shown.

Far from the structures (**Figure 7** left), the viruses appear as known from untreated samples.^[18–20] Right next to the structure (**Figure 7** center), however, the viruses appear blurred and their *z*-height is less than half of the *z*-height of the undisturbed viruses recorded further away from the structure. Within the structures, no virus assembly is recognizable. However, cloudy structures with a large *z*-height can be determined. We assume that this is an effect of the ion beam interacting with the silicon substrate and maybe some remnants from the viruses. It is well known that ion bombardment may lead to the destruction of the upper surface layers and therefore a roughening effect. The assumption of interaction of FIB with the silicon wafer is corroborated by the measurements on an FIB-structured multilayer viral system (see the Supporting Information). There, the *z*-height inside the structure is less because the interaction between the ion beam and silicon is shielded by the thicker virus layer.

Experiments with a focused electron beam (see the Supporting Information) show that the structuring of virus layers through the direct interaction of the focused electron beam with the virus layer cannot be realized with moderate energies and time periods. This is in line with Alonso et al.^[45] They integrated tobacco mosaic virus (TMV) in electron beam lithography nanostructures without destroying the viruses. This approach was thus no longer followed.

4. Conclusion

In summary, it is possible to generate laterally structured patterns of viruses with both the FluidFM and the focused ion beam method, whereas electron beam lithography does not give sufficient results. Both methods have their advantages and disadvantages. The main difference is that the FluidFM provides the negative structure of the FIB. Although the same structures can be obtained with both methods, this may require considerable additional time. FluidFM writing in addition leaves the rest of the substrate unchanged.

However, controlling FluidFM patterns is considerably more difficult than in FIB. Important parameters to be controlled are on the one hand properties of the solution such as viscosity and surface tension and on the other hand the shape, size, and concentration of the nanoparticles. These parameters determine not only the droplet formation and virus attachment to the surface, but also together with the properties of the ambient, such as

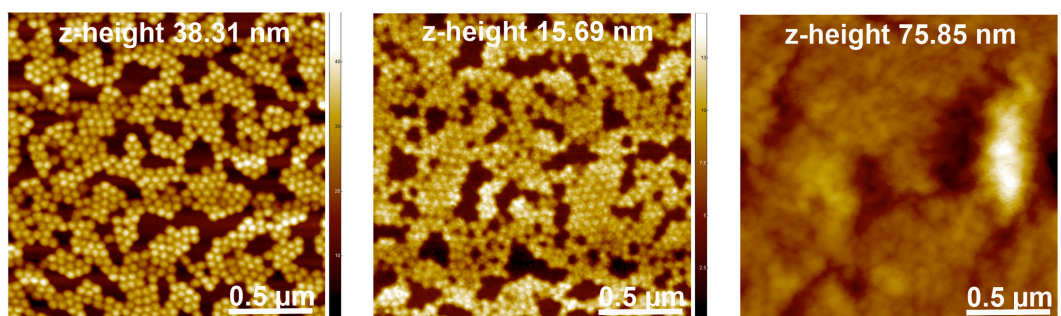


Figure 7. Scanning force microscope images of the FIB written structures into $1.0 \mu\text{g } \mu\text{L}^{-1}$ Strep-tagII TBSV; left: at a greater distance; center: directly next to a structure; right: within a structure. The images are taken on the sample with the squares.

humidity and temperature, the movement of the particles during the drying process. It was shown that the drying process plays a dominant role in the final pattern appearance. Finally, the used type of FluidFM cantilever and herewith the geometry of the contact between the aperture and substrate play an important role. If a nanopipette is used and thus the aperture is pressed onto the substrate, the viruses have to overcome the dwell force to get out of the probe. Viruses are elastic nanoparticles and can deform to overcome this very small gap between the tip apex and substrate. However, this deformation may lead to the destruction of the viruses (see Supporting Information). Thus, the use of nanopipettes is not suitable to write viral structures. In contrast, the aperture of the nanosyringe is not in direct contact with the substrate and writing is possible, but the structures lose some accuracy due to the higher diameter of the aperture (800 nm instead of 300 nm). FluidFM is thus an interesting tool to create small patterns of viruses, but pattern formation is a complex process involving a variety of parameters to be controlled.

Supporting Information

Supporting Information is available from the Wiley Online Library or from the author.

Acknowledgements

This work was supported by the Deutsche Forschungsgemeinschaft (grant numbers Zi 487/18-1 and Kr 2242/4-1). In addition, the financial support by the research center OPTIMAS is highly appreciated. The provision of the scanning electron microscope by the Nano Structuring Center Kaiserslautern, the contact angle measurement device by the IFOS Kaiserslautern as well as the viscosimeter by the IVW Kaiserslautern is highly appreciated. The authors acknowledge Bert Lägél (e-beam at the Nano Structuring Center Kaiserslautern) and Jörg Lösch (FIB-CUT at the IFOS Kaiserslautern) for performing the lithographies as well as helpful discussions.

Open access funding enabled and organized by Projekt DEAL.

Conflict of Interest

The authors declare no conflict of interest.

Data Availability Statement

The data that support the findings of this study are available from the corresponding author upon reasonable request.

Keywords

FluidFM, focused ion beam lithography, virus nanoparticles, 2D patterning

Received: April 30, 2021

Revised: June 8, 2021

Published online: July 29, 2021

- [1] A. Biswas, I. S. Bayer, A. S. Biris, T. Wang, E. Dervishi, F. Faupel, *Adv. Colloid Interface Sci.* **2012**, *170*, 2.
[2] D. Mijatovic, J. C. T. Eijkel, A. van den Berg, *Lab Chip* **2005**, *5*, 492.

- [3] J. H. Hah, S. Mayya, M. Hata, Y.-K. Jang, H.-W. Kim, M. Ryoo, S.-G. Woo, H.-K. Cho, J.-T. Moon, *J. Vac. Sci. Technol. B Microelectron.* **2006**, *24*, 2209.
[4] Z. Peng, H. Liu, *Chem. Mater.* **2016**, *28*, 1012.
[5] C. Azucena, F. J. Eber, V. Trouillet, M. Hirtz, S. Heissler, M. Franzreb, H. Fuchs, C. Wege, H. Gliemann, *Langmuir* **2012**, *28*, 14867.
[6] X. Fu, J. Cai, X. Zhang, W.-D. Li, H. Ge, Y. Hu, *Adv. Drug Delivery Rev.* **2018**, *133*, 169.
[7] M. Young, W. Debbie, M. Uchida, T. Douglas, *Annu. Rev. Phytopathol.* **2008**, *46*, 361.
[8] S.-Y. Lee, J.-S. Lim, M. T. Harris, *Biotechnol. Bioeng.* **2012**, *109*, 16.
[9] D. J. Evans, *J. Mater. Chem.* **2008**, *18*, 3746.
[10] C. Müller-Renno, V. Rink, M. Ani, M. Braun, K. Boonrod, G. Krczal, C. Ziegler, *Biointerphases* **2020**, *15*, 041009.
[11] J. N. Culver, A. D. Brown, F. Zang, M. Gnerlich, K. Gerasopoulos, R. Ghodssi, *Virology* **2015**, *479–480*, 200.
[12] C. M. Soto, B. R. Ratna, *Curr. Opin. Biotechnol.* **2010**, *21*, 426.
[13] I. Yildiz, S. Shukla, N. F. Steinmetz, *Curr. Opin. Biotechnol.* **2011**, *22*, 901.
[14] C. Koch, A. Poghossian, M. J. Schöning, C. Wege, *Nanotheranostics* **2018**, *2*, 184.
[15] S. Eiben, C. Koch, K. Altintoprak, A. Southan, G. Tovar, S. Laschat, I. M. Weiss, C. Wege, *Adv. Drug Delivery Rev.* **2019**, *145*, 96.
[16] N. F. Steinmetz, K. C. Findlay, T. R. Noel, R. Parker, G. P. Lomonosoff, D. J. Evans, *ChemBioChem* **2008**, *9*, 1662.
[17] N. F. Steinmetz, G. P. Lomonosoff, D. J. Evans, *Langmuir* **2006**, *22*, 3488.
[18] V. Rink, C. Müller-Renno, C. Ziegler, M. Braun, K. Boonrod, G. Krczal, *Biointerphases* **2017**, *12*, 05G606.
[19] A. Lüders, C. Müller, K. Boonrod, G. Krczal, C. Ziegler, *Colloids Surf. B* **2012**, *91*, 154.
[20] D. Hiller, D. König, K. Kúsová, *Phys. Status Solidi C* **2016**, *13*, 163.
[21] M. Y. Amarouch, J. El Hilaly, D. Mazouzi, *Scanning* **2018**, *2018*, 7801274.
[22] A. Meister, M. Gabi, P. Behr, P. Studer, J. Vörös, P. Niedermann, J. Bitterli, J. Polesel-Maris, M. Liley, H. Heinzelmann, T. Zambelli, *Nano Lett.* **2009**, *9*, 2501.
[23] R. R. Grüter, J. Vörös, T. Zambelli, *Nanoscale* **2013**, *5*, 1097.
[24] V. Martinez, C. Forró, S. Weydert, M. J. Aebbersold, H. Dermutz, O. Guillaume-Gentil, T. Zambelli, J. Vörös, L. Demkó, *Lab Chip* **2016**, *16*, 1663.
[25] A. Mark, N. Helfricht, A. Rauh, M. Karg, G. Papastavrou, *Small* **2019**, *15*, 1902976.
[26] T. Gerecsei, I. Erdódi, B. Peter, C. Hős, Sándor. Kurunczi, I. Derényi, Bálint. Szabó, R. Horvath, *J. Colloid Interface Sci.* **2019**, *555*, 245.
[27] P. Saha, T. Duanis-Assaf, M. Reches, *Adv. Mater. Interfaces* **2020**, *7*, 2001115.
[28] L. Hofherr, C. Müller-Renno, C. Ziegler, K. G. Blank, *Plos One* **2020**, *15*, e0227395.
[29] T. Schlotter, S. Weaver, C. Forró, D. Momotenko, J. Vörös, T. Zambelli, M. Aramesh, *ACS Nano* **2020**, *14*, 12993.
[30] M. Aramesh, C. Forró, L. Dowling-Carter, I. Lütchefeld, T. Schlotter, S. J. Ihle, I. Shorubalko, V. Hosseini, D. Momotenko, T. Zambelli, E. Klotzsch, J. Vörös, *Nat. Nanotechnol.* **2019**, *14*, 791.
[31] Y. Cui, X. Lyu, L. Ding, L. Ke, D. Yang, M. Pirouz, Y. Qi, J. Ong, G. Gao, P. Du, R. I. Gregory, *Nature* **2021**, *593*, 602.
[32] T. J. Morris, T. Joelson, B. Strandberg, K. Tomenius, L. Akerblom, P. Oxelfelt, *J. Gen. Virol.* **1997**, *78*, 1213.
[33] A. Escarpa, M. Pumera, *Electrophoresis* **2017**, *38*, 2771.
[34] A. J. Olson, G. Bricogne, S. C. Harrison, *J. Mol. Biol.* **1983**, *171*, 701.
[35] P. Q. Hearne, D. A. Knorr, B. I. Hillman, T. J. Morris, *Virology* **1990**, *177*, 141.
[36] I. K. Robinson, S. C. Harrison, *Nature* **1982**, *297*, 563.

- [37] A. Saftics, B. Türk, A. Sulyok, N. Nagy, T. Gerecsei, I. Szekacs, Sándor. Kurunczi, R. Horvath, *Langmuir* **2019**, 35, 2412.
- [38] J. Ventrici de Souza, Y. Liu, S. Wang, P. Dörig, T. L. Kuhl, J. Frommer, G.-y. Liu, *J. Phys. Chem.* **2018**, 122, 956.
- [39] D. Rimmel, 3D Bau mit Pflanzenviren, Master Thesis, Kaiserslautern **2020**.
- [40] X. Zhong, A. Crivoi, F. Duan, *Adv. Colloid Interface Sci.* **2015**, 217, 13.
- [41] C. H. Chon, S. Paik, J. B. Tipton, K. D. Kihm, *Langmuir* **2007**, 23, 2953.
- [42] C. Sadek, P. Schuck, Y. Fallourd, N. Pradeau, C. Le Floch-Fouéré, R. Jeantet, *Dairy Sci. Technol.* **2015**, 95, 771.
- [43] D. Brutin, *Colloids Surf. A* **2013**, 429, 112.
- [44] R. D. Deegan, *Phys. Rev. E* **2000**, 61, 475.
- [45] J. M. Alonso, T. Ondarçuhu, A. M. Bittner, *Nanotechnology* **2013**, 24, 105305.